Mapping of debris-covered glaciers in the Garhwal Himalayas using ASTER DEMs and thermal data

Bhambri, R ; Bolch, T ; Chaujar, R K

Abstract: Mapping of debris-covered glaciers using remote-sensing techniques is recognized as one of the greatest challenges for generating glacier inventories and automated glacier change analysis. The use of visible (VIS) and near-infrared (NIR) bands does not provide sufficient continual information to detect debris-covered ice with remote-sensing data. This article presents a semi-automated mapping method for the debris-covered glaciers of the Garhwal Himalayas based on an Advanced Spaceborne Thermal Emission and Reflection Radiometer (ASTER) digital elevation model (DEM) and thermal data. Morphometric parameters such as slope, plan curvature and profile curvature were computed by means of the ASTER DEM and organized in similar surface groups using cluster analysis. A thermal mask was generated from a single band of an ASTER thermal image, while the clean-ice glaciers were identified using a band ratio based on ASTER bands 3 and 4. Vector maps were drawn up from the output of the cluster analysis, the thermal mask and the band ratio mask for the preparation of the final outlines of the debris-covered glaciers using geographic information system (GIS) overlay operations. The semi-automated mapped debris-covered glacier outline of Gangotri Glacier derived from 2006 ASTER data varied by about 5% from the manually outlined debris-covered glacier area of the Cartosat-1 high-resolution image from the same year. By contrast, outlines derived from the method developed using the 2001 ASTER DEM and Landsat thermal data varied by only 0.5% from manually digitized outlines based on Indian Remote Sensing Satellite (IRS)-1C panchromatic (PAN) data. We found that post-depositional sedimentation by debris flow/mass movement was a great hindrance in the fully automated mapping of debris-covered glaciers in the polygenetic environment of the Himalayas. In addition, the resolution of ASTER stereo data and thermal band data limits the automated mapping of small debris-covered glaciers with adjacent end moraine. However, the results obtained for Gangotri Glacier confirm the strong potential of the approach presented.

DOI: https://doi.org/10.1080/01431161.2010.532821

BHAMBRI, R., BOLCH, T., CHAUJAR, R.K. (2011): Automated mapping of debris-covered glaciers in the Garhwal Himalayas using ASTER DEMs and multi-spectral data. *International Journal of Remote Sensing* 32(23): 8095-8119. doi: 10.1080/01431161.2010.532821, accepted manuscript.

Mapping of Debris-covered Glaciers in the Garhwal Himalayas using ASTER DEMs and Thermal Data

R. BHAMBRI*†, T. BOLCH‡§, R. K. CHAUJAR¶
†Central Soil Salinity Research Institute, Karnal-132001, Haryana, India,
‡Institut für Kartographie, Technische Universität Dresden, 01069 Dresden, Germany,
§Geographisches Institut, Universität Zürich, Switzerland,
¶Wadia Institute of Himalayan Geology, Dehradun-248001, India

Abstract

Mapping of debris-covered glaciers using remote sensing techniques is recognized as one of the greatest challenge for generating glacier inventories and automated glacier change analysis. The use of visible (VIS) and near infrared (NIR) bands does not constantly provide sufficient information to detect the debris-covered ice with remote sensing data. This paper presents a semi-automated mapping method for the debris-covered glaciers of the Garhwal Himalayas based on an ASTER DEM and thermal data. Morphometric parameters such as slope, plan curvature and profile curvature were computed by the means of the ASTER DEM and organized in similar surface groups using cluster analysis. A thermal mask was generated from a single band of an ASTER thermal image, while the clean-ice glaciers were identified using a band ratio based on ASTER bands 3 and 4. Vector maps were drawn up from the output of the cluster analysis, the thermal mask and from the band ratio mask for the preparation of final outlines of debris-covered glaciers using GIS overlay operations. The semi-automated mapped debris-covered glacier outline of Gangotri Glacier derived from 2006 ASTER data varies ~5% from the manually outlined debris-

* Corresponding author. now at: Center for Glaciology, Wadia Institut…
Email: rakeshbhambri@gmail.com

covered glacier area of the Cartosat-I high resolution image from the same year. By contrast, outlines derived from developed method using 2001 ASTER DEM and Landsat thermal data vary only 0.5% from manually digitized outlines based on IRS IC-PAN data. We found that post-depositional sedimentation by debris flow/mass movement was a great hindrance in the full automated mapping of debris-covered glaciers in the polygenetic environment of the Himalayas. In addition, the resolution of ASTER stereo data and thermal band limits automated mapping of small debris-covered glacier with adjacent terminal moraine. However, the results obtained from the Gangotri Glacier confirm the strong potential of the presented approach.

1 Introduction

Glaciers are composed of snow, ice, water and rock/debris materials which move slowly down a gradient. The valley glaciers are often covered with varying amounts of debris (also called “scree”) consisting of dust, silt, sand, gravel, cobble and boulders in various mountain ranges including the Himalayas (Fushimi *et al.* 1980, Shroder *et al.* 2000, Bolch *et al.* 2008a, Hambrey *et al.* 2008, Hewitt 2009), the Andes (Racoviteanu *et al.* 2008) and the Alps (Paul *et al.* 2004, Ranzi *et al.* 2004, Bolch and Kamp 2006). This indicates shrinkage of glaciers that leads to the deposition of unstable debris in ablation areas. Several studies reported that debris cover has been increased over time concomitant with glacier shrinkage in the Himalayas (e.g. Iwata *et al.* 2000, Bolch *et al.* 2008a), the Alps (Bolch and Kamp 2006, Kellerer-Pirklbauer 2008) and the Caucasus (Popovnin and Rozova, 2002, Stokes *et al.* 2007). The debris-covered (also called “debris-mantled” or “moraine-covered”) glaciers have been recognized as an efficient sediment transport agent in cold mountain environment (Kirkbride 1995). This sediment can be transported by the glacier on its surface (supraglacial), within glacier ice (englacial), as well as below (subglacial) the glacier ice (Small 1987). The debris is delivered by mass movements activities such as rockfalls, rock avalanches, debris flows, and snow/ice avalanches from adjacent lofty slopes on the glacier surfaces (Shroder *et*

al. 2000, Fort 2000, Hewitt 2009) due to slope instabilities in the high-mountains (Kääb *et al.* 2006, Fischer *et al.* 2006) and transfer of debris from the glacier bed to the surface along shear planes. The debris cover on glaciers has been considered as the key problem in glaciology due to the following reasons.

(1) The assessment of debris-covered is crucial for glacier mass balance, glacier rheology and glacier dynamics. Debris-covered on glaciers greatly affects their rate of ablation. For instance, thick debris can reduce ablation up to 40% (Mattson 2000, Pelto 2000). In result, glaciers covered with thick debris react more slowly to climatic changes (Benn and Evans 1998, Mattson 2000).

(2) The thick debris-covered often hampers the detection of the actual terminus, and the reaction of the glacier to climate influences can be recognized mainly through the downwasting process (Bolch *et al.* 2008b, Schmidt and Nüsser 2009).

(3) Several thick debris-covered glaciers contain stagnant ice parts at their fronts and respond with greater interlude to climate fluctuations than clean ice glaciers. (Bolch *et al.* 2008a, 2008b, Schmidt and Nüsser 2009, Racoviteanu *et al.* 2009).

(4) Supraglacial lakes can develop on the ablation zone of debris-covered glaciers rather than clean ice glaciers. These lakes can join to form a larger lake (Benn *et al.* 2000, Reynolds 2000, Bolch *et al.* 2008b, Komori 2008). The water in these lakes can drain away in a matter of minutes, thus triggering a glacier hazard of catastrophic dimensions.

In addition, the water discharge from the debris-covered Himalayan glaciers contributes to a certain amount to the overall river runoff (Immerzeel *et al*. 2010). It is therefore essential to monitor debris-covered glaciers at regular intervals. However, field based monitoring of glaciers is time-consuming and poses the potential risk of long stays in remote, extensive rugged, and extreme weather conditions, which in turn has financial implications as well. The recent progress in remote

sensing and GIS techniques offer great potential for mapping and monitoring of large glacier coverage concurrently (Paul *et al.* 2002, Bhambri and Bolch 2009, Bolch *et al.* 2010).

Glacier and snow mapping is based on the fact that snow and ice presents high reflectance in the visible and near infrared region (VIS and NIR) as compared to the short-wave infrared (SWIR) region of the electromagnetic spectrum. This information has been applied for clean-ice glaciers mapping using band ratio, NDSI and supervised classification (Sidjak and Wheate 1999, Albert 2002, Paul *et al.* 2002, Bolch and Kamp 2006, Raup *et al.* 2007, Andreassen *et al.* 2008, Racoviteanu *et al.* 2008). However, these image-processing techniques have been appeared ineffective to map debris-covered glaciers due to the similar spectral signature of surrounding rocky moraines and glacier fore-fields (Bishop *et al.* 2001, Quincey *et al.* 2005, Raup *et al.* 2007). For this reason, glacier inventories based on remote sensing in the Himalayas has been delineated manually debris-covered glaciers from satellite images (Dobhal and Kumar 1996, Kulkarni and Suja 2003, Kulkarni *et al.* 2005, 2007, Berthier *et al.* 2007, Bolch *et al*. 2008a). Nevertheless, this method is time consuming for larger areas and its accuracy depends on the expert's ability to efficiently identify and recognize glacier terrain features on satellite imageries.

Therefore, previous studies have been used some inventive methodologies for debris-covered glacier mapping such as: (1) pixel based image processing techniques including supervised classification on topographically corrected reflectance images (Shukla *et al.* 2009), artificial neural networks (ANN) (Bishop *et al.* 1999, Shroder *et al.* 2000) and Normalized Difference Glacier Index (NDGI) (Keshri *et al.* 2009); (2) morphometric parameters such as slope, plan and profile curvature (Bishop *et al.* 2001, Bolch and Kamp 2006); (3) multi criteria technique including multispectral image classification (glacier ice, vegetation), neighborhood analysis (connection to glacier ice), and change detection (Paul *et al.* 2004), and morphometric parameters with optical and thermal datasets (Bolch *et al.* 2007) and optical–thermal remote sensing data with inputs from geomorphometric parameters (Shukla *et al.* 2010); (4) difference in thermal properties of glacier

ice, snow and debris-covered ice using thermal satellite images (Taschner and Ranzi 2002, Ranzi *et al.* 2004, Mihalcea *et al.* 2006, 2007); and (5) benchmarking optimal classifiers (Brenning 2009). However, almost all the discussed methods are region-specific, not universally established and optimized for a small region. In contrast, the method proposed by Brenning (2009) is suitable for detecting potential niches for rock glaciers and debris-covered glaciers over an entire mountain range. The accuracy, however, is too low for change detection. All this can be assumed due to differences in regional/local landscape conditions such as (1) different size, shape and height of debris-covered glacier snouts, (2) vegetation cover, (3) surface ponds, (4) characteristics of debris-cover (medial moraine vs. thick debris cover on whole tongue), and (5) the amount of debris cover on ablation zone. It is noteworthy that there has not yet been a successful attempt at automated or semi-automated mapping of debris-covered Gangotri Glacier and other Garhwal Himalayan glaciers.

The principal objectives of this study are: (1) the demonstration of a further developed multiple criteria technique for debris-covered glacier mapping based on Bolch and Kamp (2006) and Bolch *et al.* (2007) using cluster analysis of morphometric parameters such as slope, plan curvature, profile curvature, band ratio technique, thermal band information derived from ASTER data, and evidence from fieldwork. This study focused on different types of debris-covered glaciers such as without end moraine and glacier with adjacent end moraine at wider scale in the Garhwal Himalayas; and (2) the validation and evaluation of the presented automated mapping method of debris-covered glaciers based on an additional ASTER image, the thermal band of Landsat ETM+, and high resolution imagery

Figure 1 around here

2 Study Area

Gangotri Glacier, the largest glacier in the Garhwal Himalayas (length: ~30 km, area: ~130 km^2) was selected as the primary research area for present study. It originates from the Chaukhamba group of peaks (~7058m) and flows in northwesterly direction up to Gaumukh (snout of Gangotri; figure 1). The adjacent glaciers such as the Raktavan (~13 km, ~32 km^2) and Chaturangi (~22 km, ~64 km^2) were chosen as secondary study sites for examining the developed technique of mapping of debris-covered glaciers. Since all three glaciers are of great magnitude (very large in length and size), the smaller, debris-covered Chorabari Glacier (~7 km, ~5.4 km^2) was also selected for testing the developed approach. Chorabari Glacier is a south-facing debris-covered glacier which is the source of Mandakani River (one tributary of the Ganga River). The Gangotri Glacier system is a cluster of several large and small glaciers. Swachand, Maindi, and Ghanohim are some of the active tributary glaciers which are still connected to the main Gangotri Glacier and contribute to the mass balance of the main glacier. Raktavan Glacier has been detached from the main Gangotri Glacier. Chaturangi Glacier was a part of the main Gangotri Glacier until 1962, as presented in the Survey of India topographic map. Naithani *et al.* (2001) reported that Chaturangi Glacier has retreated 250 m from 1971 to 1999.

Figure 2 around here

The debris on the on the Gangotri, Raktavan and Chaturangi glaciers reflects the local geology dominated by granite, granitic gneiss and sheared granitic gneiss (Chaujar et *al.* 1993). Visual interpretation of ASTER satellite image indicates that the surface of Gangotri Glacier is covered by debris from its terminus to about 19 km upstream where Swachand Glacier, a tributary glacier, joins Gangotri Glacier. The snout of the Gangotri Glacier and its surrounding areas are comprised of very rugged terrain, and the ablation zone of Gangotri Glacier is covered with supra-glacial ponds, ice fractures/crevasses and supra-glacial debris (figure 2). To our knowledge no study on the debris thickness of these glaciers exists so far. In the Himalayas, several glaciers have

a large cave at their termini. In the case of Gangotri Glacier, the snout cave height was estimated to be 75 m (Barnard *et al.* 2004). Chorabari Glacier does not have one and the end moraine is a source of complexity around its snout area (figure 3 and 2(*a*))

Figure 3 around here

3 Data Sources

3.1 Field data

GPS readings were acquired using a hand-set Garmin Etrex GPS unit due to unavailability of expensive DGPS equipment in navigation mode on pro-glacial areas (Gangotri temple) up to glaciated areas during the visit to Tapoban in October 2007. However, a disadvantage of the navigation mode GPS is that it is not differentially accurate. Nevertheless, these hand-set Garmin GPS instruments are a useful substitute if no other source of GCPs is available and vertical accuracies are in the order of ±15 m in mountainous terrain (Racoviteanu *et al.* 2007). In addition, horizontal accuracies of ±3.9 m are possible (Ackerman *et al.* 2001). Vertical accuracy of ±10 to 15 m was estimated, displayed by GPS screen depending on the number of satellite signals it receives.

Table 1 around here

3.2 Satellite data and topographic map

Various medium- and high-resolution satellite images such as ASTER, ETM+, Cartosat-I, IRS-IC PAN were evaluated at the end of the ablation season. Five images without fresh snow cover were selected (table 1). Two Level 1A ASTER scenes (September 2001 and October 2006) were acquired with all of its 14 bands from the Land Processes DAAC at EROS Data Center.

Fortunately, our area of interest was almost cloud-free in both ASTER images. One cloud-free ETM+ thermal band image from October, 1999 was downloaded from the Global Landcover Facility (GLCF, www.landcover.org). The high-resolution Indian panchromatic satellite data Cartosat-I from September, 2006 at 2.5 m resolution and IRS IC-PAN data of October 2001 at 5.8 m resolution was acquired from National Remote Sensing Centre (NRSC, http://www.nrsa.gov.in) for the evaluation of semi-automated outlines of debris-covered glacier area derived from ASTER data. Cartosat-I images have been used successfully for glacier mapping and elevation change studies (Bahuguna 2008). Cartosat-I data was obtained in 10-bit radiometric resolution which helps in the interpretation of complex polygenetic glacier landscape due to better contrast than other available IRS-IC and ID PAN data. The Cartosat-I data covers the whole debris-covered area of Gangotri Glacier but only parts of Raktavan and Chaturangi Glaciers due to limited swath (~27 km). The topographic map 53N/1 (1:50000) is used as a base map, which was prepared by the Survey of India in the 1960s using aerial photographs with limited fieldwork.

3.3 ASTER Digital Elevation Model (DEM)

Terra ASTER is the most economical optical sensor which covers a 60 km wide ground track at a 15 m spatial resolution (Toutin 2008), which is the primary source of DEM generation under the GLIMS Project (Kargel *et al.* 2005, Raup *et al.* 2007). The ASTER sensor offers image data in 14 visible, near-infrared, short wavelength infrared and thermal infrared spectral bands. Stereo image data are accessible in Band 3, which comes in near-infrared wavelength region from 0.78 to 0.86 µm, using both nadir and aft-looking scene. Terra ASTER offer along track stereo capability with quasi-simultaneous image acquisition, while the other sensors (e.g. SPOT 4) offer across-track acquisition where the time lag in the acquisition may cause problems (e.g. due to clouds, different atmospheric conditions). Images generated from the nadir and aft -looking scene yield a B/H ratio of 0.6. It is ideal for generating DEMs through automated techniques. Due to stereopairs of

consistent quality Terra ASTER has been recognized and well suitable for DEM generation using automated stereocorrelation techniques (Kamp *et al.* 2005, Toutin 2008).

Figure 4 around here

The ASTER DEMs for 2001 and 2006 were generated from stereo 3N and corresponding 3B band based on major steps including: ground control points (GCPs) collection, transformation to epipolar images, parallax-matching, and parallax to DEM using ENVI 4.2 software. Total 11 GCPs and 9 GCPs were used for 2006 and 2001 ASTER scenes respectively. The GCPs were acquired from two sources: Survey of India topographic map and GCPs collected during fieldwork limited to the proglacial area of Gangotri Glacier. In addition, 129 tie points (TPs) and 152 TPs were used for better image matching for 2006 and 2001 ASTER scenes, respectively. Stable streams junctions, road river junctions, and lake-stream junction were used for TPs and GCPs assuming no changes occurred according to time in GCPs locations on the ground. The DEMs were generated with a resolution of 30 m. ASTER derived DEMs (30 m spatial resolution) have been validated at mountainous regions (Kääb 2002, Kamp *et al.* 2005, Racoviteanu *et al.* 2007). The 30 m spatial resolution of ASTER DEMs is also recommended to avoid avoids noise in the comparison of the 15 m spatial resolution (Toutin 2008). The objective of using a second DEM for the same area was testing and validating the proposed methodology for debris-covered glacier mapping. Cloud-covered areas were manually removed from the DEM based on clip algorithm using ArcGIS. The raw DEMs were promising, but 2006 ASTER DEM had four unnatural peaks in the accumulation zone of Gangotri Glacier covering an area less than 0.02 km² (figure 4). These unnatural peaks are one key problem with ASTER DEMs in high mountain terrain (Toutin 2008). These peaks were eliminated manually through clip by mask algorithm using ArcGIS and the resulting holes were filled by interpolation method using the SAGA software. The vertical accuracy of the final ASTER

DEMs was evaluated using GPS values obtained during a field campaign. Elevation values of 2006 ASTER DEM vary from -30m to +31m with respect to GPS fieldwork elevation, whereas in the case of 2001 ASTER DEM elevation values, the variation is between -164m to +68m with respect to GPS fieldwork readings. Moreover, SRTM DEM elevation values vary -63m to + 28m with respect to GPS values. RMSE was found to be ±21m and ±42m for 2006 and 2001 ASTER DEM respectively, and ±27m for SRTM data, which is acceptable in rugged terrain and comparable with ASTER DEMs in rugged terrain in the Swiss Alps and Andes (Kääb 2002, Racoviteanu *et al.* 2007). ASTER images of 2006 and 2001 were orthorectified using their resultant ASTER DEMs. In addition, ASTER DEM (2006) was also utilized for orthorectification of Cartosat-I, IRS IC-PAN, and ETM+ thermal images unavailability of same base DEM. Satellite images orthorectified by the similar base DEM data is advisable in the rugged terrain and assured that no additional error is introduced due to different orthorecitfication. The number of GPSs is crucial for accuracy of orthorecitfication of high resolution data (Thakur *et al.* 2008). Hence, we used around 50 GCPs for orthorectification of all the images. We found 10 and 15 m RMSE for high resolution Cartosat-I and IRS IC-PAN images respectably which is acceptable in rugged terrain.

Figure 5 around here

4. Automated mapping of debris-covered glaciers

4.1 Developed approach

In this section, the developed methodology is described stepwise for debris-covered mapping based on our multiple criteria approach. The detailed methodology is illustrated in figure 5. The semi-automated approach is a further development based on Bolch and Kamp (2006) and Bolch *et al.* (2007) using a 2006 ASTER DEM and ASTER thermal data.

4.1.1 **Morphometric parameter mapping** – Geomorphometric maps such as slope, plan curvature and profile curvature were computed after the postprocessing of ASTER DEMs using a local morphometric tool of the SAGA software (Conrad *et al.* 2006) which is based on the Zevenberg and Thorne (1987) approach.

4.1.2 **Cluster analysis** - Plan and profile curvature were combined by cluster analysis and placed in ten categories with similar surface characteristics (figure 6(*b*)). Iterative minimum distance statistical technique proposed by Forgy (1965) was applied for cluster analysis using a wizard-based tool provided by SAGA. A cluster analysis was conducted again on slope and the previous results of both curvatures and once more rearranged into ten categories (figure 6(*c*)).

Figure 6 around here

4.1.3 **Reclassification** - Three out of ten categories were visually selected and reclassified which covered Gangotri Glacier (figure 6(*d*)). The reclassified output was then converted into a vector polygon map and the area of interest (e.g. Gangotri Glacier) was selected manually (figure 6(*e*) and (*f*)). However, the result also covered some part of the lateral moraine near the accumulation zone of Ghanohim Glacier. We found that this area can be removed using information derived from the thermal band of ASTER.

4.1.4 **Single thermal band thresholding** - Pixel values of single thermal band 12 of ASTER for thresholding procedure (figure 7) were carefully checked. Taschner and Ranzi (2002) also used band 12 of ASTER for debris-covered glacier mapping. 5.9 to 7.5 were used as a threshold value to generate a thermal mask in binary image format. The result derived from the thermal mask was then converted into a vector polygon map and the area of interest was selected manually. The thermal mask also misclassified a pro-glacier area near the snout of Gangotri Glacier probably due

to its equally cold temperature. Similar results were presented by Shukla *et al.* (2010) during the mapping of Samudra Tapu Glacier based on ASTER thermal data.

Figure 7 around here

4.1.5 **Clean glacier-ice mapping** - The Band ratio method based on NIR and SWIR bands (e.g. ASTER band 3 and 4) is widely used for clean-ice glacier mapping (Paul *et al.* 2002, Bolch and Kamp 2006, Paul *et al.* 2009). The clean glacier-ice mask was generated in binary image format based on this band ratio using a carefully selected threshold value 1.0 and converted into a vector polygon map. We found that some dark shadow areas were also misclassified as glacier ice. These misclassified areas were manually improved from the vector polygon. (figure 8). However, it also covered the surrounding clean glacier ice of Satopanth and Bhagirathi Kharak Glacier. The ice divide was identified via visual inspection of ASTER DEM with hillshade effect and ASTER bands 321 and then manually digitized. This vector layer of the ice divide was used for the segregation of Gangotri, Raktavan and Chaturangi Glacier polygons from their surrounding glaciers based on the simple overlay clip algorithm of ArcGIS. The clean ice layer is important for the correct debris-cover glacier mapping. Each glacier has an accumulation area without debris-cover. Hence, only those classified areas which are connected to the clean ice layer were selected as a debris-cover glacier by location tool.

Figure 8 around here

4.1.6 **Overlay operations** - We found that misclassified pro-glacier area near the Gangotri snout from thermal threshold can be removed using plan, profile curvature, and slope information. This is based on the fact that the end of the terminus has a steeper slope than is direct forefield. Hence, the

transition is characterised by a bend which can be detected using slope and curvature information (Bolch and Kamp 2006). Therefore for the generation of the final outline of the debris-covered glaciers, the overlay operation 'intersect' was applied on the vector map layer derived from cluster analysis and the thermal mask vector map layer using ArcGIS. The intersect method played a vital role in the elimination of additional area near the snout of Gangotri Glacier derived from thermal threshold, and lateral moraine area near Ghanohim Glacier derived from reclassified cluster output of plan, profile curvatures and slope. However, the transitional zone area of clean-ice and debris-covered area was misclassified as debris-covered area possibly due to two reasons (1) no change occurred in slope near the transitional zone area of clean-ice and debris-covered area and (2) the spatial resolution of ASTER thermal data limits to differentiate clean-ice and debris-covered area at their junctions. These areas were removed from the clean-ice vector polygon map using the erase function of the overlay operation (figure 9). Some small polygons were found existing outside Gangotri, Raktavan and Chaturangi Glaciers. As a final step, these misclassified small polygons were removed using an area threshold of less than 0.25 km². This threshold is justified by the fact that debris-covered glaciers are usually larger than clean ice glaciers and almost no debris occurs on glacierets and small hanging glaciers. A threshold of 0.1 km² for clean-ice glaciers was used for several glacier inventories, e.g., for the Swiss Alps (Paul *et al.* 2002).

4.2 Validation and evaluation of automated techniques

The technique discussed above was tested for semi-automated mapping of debris-covered glaciers in 2001 using the 2001 ASTER DEM and Landsat thermal information. A similar methodology was applied for validation but, in this case, Landsat thermal band was used, as Landsat thermal band offered better resolution (60m) than ASTER thermal band (90m). However, in this case, 92 to 115 were used as a threshold value to generate thermal mask in binary image format. The ASTER band ratio 3 / 4 (NIR/SWIR) used for clean glacier ice mapping and 8.0 was used as threshold for the

generation of binary image from this ratio image. Similarly, the number of selected cluster groups was changed for the generation of reclassified output. In this case, two categories out of ten were selected which cover Gangotri Glacier.

In addition, the debris-covered areas of Gangotri, Raktavan and Chaturangi Glaciers were delineated manually on high-resolution Cartosat-I and IRS IC-PAN images based on visually interpretation for evaluation of the developed approach. We used several indicators for the correct delineation as the existence of supraglacial lakes, sign of movements such as a rough texture in contract to the moraines or creeks which drain from the glacier snout. We also enhanced the images using linear technique and cross checked the results during field verification at some accessible areas. Manual delineation of glaciers on high-resolution images is a time-consuming process, but it aids in finding out to what extent the automated outline varied from the manually delineated debris-covered glacier outline.

Figure 9 around here

5 Results

The semi-automated debris-covered glacier outline of Gangotri Glacier derived from 2006 ASTER data was 5.04% smaller than the manually outlined debris-covered glacier area from the Cartosat-I high-resolution image of the same year. Further results are summarized in the table 2. The major problem occurs near the transitional zone between the ablation and accumulation zones near the tributary Ghanohim Glacier, where a debris-covered strip about 2 km long and 80m wide was not mapped using this technique (figure 9). The semi-automated debris-covered glacier outlines derived from 2001 ASTER DEM and Landsat thermal data vary only 0.5% from manually digitized outlines based on IRS IC-PAN data.

Table 2 around here

Semi-automated outlines of debris-covered Chaturangi Glacier varies 3.96% with respect to manually digitized debris-covered outlines on 2006 ASTER data whereas in the case of 2001, semi-automated outlines derived from morphometric parameters based on ASTER DEM and thermal band of Landsat varies 5.23% area in comparison to 2001 PAN data. Also in this case, the semi-automated derived area was smaller than the manual delineated area. We found that thermal band could not significantly differentiate the debris-covered ice with its surrounding moraines in case of Chaturangi and Raktavan Glaciers due to shadow area which is attributed to the location of both glaciers from east to west.

Figure 10 around here

Results of Raktavan and Chaurabari Glaciers were only partly satisfactory. Glacier outlines derived from reclassify cluster analysis based on both 2001 and 2006 ASTER DEM had not captured the upper part of debris-covered ice of Nilamber Glacier, a tributary glacier of Raktavan Glacier (figure 10). The semi-automated glacier outline of Raktavan Glacier of 2006 varies 10.75% with manually digitized outlines from ASTER 2006 data. Similarly semi-automated glacier outline of 2001 varies 11% by from manually digitize outlines of 2001 PAN data. Also, the results of Chorabari Glacier had larger uncertainties. The present technique could not detect the snout of Chorabari Glacier and could not differentiate the end moraine from its snout area. This suggests that the resolution of the ASTER DEM was too coarse to represent the relief information of glacier terrain which would be needed for a correct delineation.

The results about cluster analysis of slope, plan and profile curvature were promising in the case of largest Gangotri Glacier. However, near Bhagirathi peaks results of reclassified cluster analysis also covered some part of lateral moraine. Visual interpretation of Cartosat-I data suggest that post depositional work by mass-movement activity covered the lateral moraine up to glacier

valley bed which was not detected by ASTER DEM (figure 11). We also noticed post depositional mass-movement activity on the lateral moraine during the field work.

Figure 11 around here

6 Discussion

6.1 Comparison with other studies

Slope is the key morphometric parameter for the intended purpose. It assists in the delineation of a debris-covered snout where terminal moraines do not exist due to discontinuity in slope between a large snout and the pro-glacier area. However, the threshold values differ depending on glacier type and height of snout cave, 'e. g.', it varies between 12° for Khumbu Glacier/Himalayas (Bolch *et al.* 2007), 24° for Oberaletschgletscher/Swiss Alps (Paul *et al.* 2004), less than 15° for Samudra Tapu Glacier/Himachal Himalayas (Shukla *et al.* 2010) and 18° for Gangotri Glacier/Garhwal Himalayas (figure 12). The visual inspection on high resolution datasets and field work confirm the great relevance of thresholding of slope method for detection of debris-covered snout cave. Previous glacier mapping studies on the Himachal Himalayas assumes that grass cover seen in the months of August and September, on terminal moraine can be used as a clue to manually delineate debris-covered glaciers (Kulkarni *et al.* 2005, 2007). However, this technique was ineffective in case of the heavily debris-covered Chorabari Glacier, as the lateral moraine would also be delineated as a glacier (figure 2). We have not observed vegetation in the lower part of the ablation zone during fieldwork at Chaurabari Glacier in the months of August and September 2006. A Principal component analysis (PCA) was performed on ASTER data for mapping of the debris-covered area of Gangotri Glacier (Ahmad and Hasnain 2004). However, this technique also includes the pro-glacial area and lateral moraines. This indicates that the method is promising but rather crude, and

if no improvements are made then it is not sufficiently be precise. Furthermore, Brovey transformation technique was performed for identification of the snout and debris-covered ice of Gangotri Glacier using IRS LISS III and IRS IC-PAN data (Bahuguna *et al.* 2004). In addition, Gangotri Glacier has been mapped based on the Landsat TM band combination of 4, 5 and 7 (Philip and Ravindran 1998). These techniques are appropriate for manual delineation of the debris-covered tongue based on visual interpretation. The proposed semi-automated method presented here is easy to perform and based on the general overlay operations which can be found in currently available GIS software. The error matrix generated by Shukla *et al.* (2009) based on supervised classification reveals that 17% pixels of other categories has been misclassified as mixed ice debris (MID). Keshri *et al.* (2009) estimated 90% and 94% producer's and user's accuracy respectively for debris class. However, this debris class also misclassified rocky cliffs face which was not considered as a separate class during validation. Previous studies such as Taschner and Ranzi (2002), Bishop *et al.* (1995), (Keshri *et al.* 2009) and Shukla *et al.* (2009; 2010) covered only one glacier for their proposed methods whereas the presented approach has been attempted on several glaciers in Bhagirathi basin. In addition, Keshri *et al.* (2009) and Shukla *et al.* (2009; 2010) present no comparison with high resolution satellite data and field investigation.

6.2 Uncertainties in study

Our study includes various data sources at different spatial and temporal resolutions. Thus evaluation of uncertainties of study is crucial. Resources of ambiguity in our study occur from: (1) processing errors associated with DEM generation from stereo ASTER data (2) ortho-rectification of satellite images (3) visual misclassifications.

The present study utilizes automatic module of ENVI 4.2 for ASTER DEM generation. This module can generate relative DEMs without GCPs, as well as absolute DEMs with GCPs based on

satellite altitude information. The previous studies suggest that the planimetric and elevation absolute accuracy can be achieved ±30 m and ±15 m respectively using ENVI (Toutin 2008). The RMSEz of the ASTER DEM (2006) with the comparison to the GPS readings is 21 m. We estimate the vertical accuracy of GPS points is ~15 m (section 3.1) as suggested by Racoviteanu *et al.* (2007), this reveals an absolute vertical accuracy of 21 m ±15 m for ASTER (2006) DEM and similarly 41 m ±15 m for ASTER (2001) DEM. The resolution of ASTER DEM (30 m) is show ineffective to identify glacial landscape complexity near the snout of highly debris-covered Chorabari Glacier. However, the present technique successfully differentiates the debris-covered snout area of the Gangotri and Raktavan Glaciers from their surrounding lateral moraines, which is the major contribution of this study. This underlines the strong potential of this proposed approach for the mapping of a debris-covered glacier tongue.

The present study includes multi-temporal coarse resolution (e.g. ASTER thermal band on 90 m grid spacing) to high resolution images (Cartosat-I on 2.5 m grid spacing). The ortho-rectification of these images is very difficult in the undulating Himalayan terrain. Similar DEM base with high resolution grid spacing is recommended for ortho-rectification of high-resolution images (Toutin 2004). In addition an inappropriate DEM in term of grid spacing can generate artifacts for linear features with high-resolution images principally over high relief areas. Cartosat-I and IRS PAN satellite images orthorectification RMSE show slight high error i.e. 10 m and 15 m respectively. However, overlay of satellite images suggests that these orthorectified images can be utilized for integration of different satellite datasets for overlay operation, registration, comparison and combine in a GIS. We notice that selection of GCPs and their number is crucial for orthorectification of Cartosat-I and IRS PAN satellite images..

Comparison between the glacier boundaries of Gangotri Glacier derived from our developed approach using ASTER (2006) and glacier outline derived from high resolution Cartosat-I (2006)

suggests an uncertainty of about ±5 %. Debris-covered glacier delineation from single band Cartosat-I and IRS PAN satellite images need interpreter efficiency of identification of glacial features. Image enhancement of 10 bit data of Cartosat-I is appear to supportive in distinguish glacial features. We also enhanced the images using linear technique and cross checked the results during field verification at some areas. The uncertainty based on a buffer method (Granshaw and Fountain 2006, Bolch et al. 2010) suggests ±2.2 % mapping error for Cartosat-I data. This reveals a total absolute mapping uncertainty is about ±5.4 % from developed semi-automatic approach based on ASTER (2006) after the validation from Cartosat-I (2006).

6.3 Constraints and potentials

Depositional works by other geomorphic processes such as debris flow/mass movement are a great hindrance in the automated mapping of debris-covered glaciers. The debris-covered boundaries could not been detected accurately by the morphometric parameters derived from the ASTER DEM in some instance due to post depositional activity (Figure 11). The post-depositional sedimentation by mass movement activity is a commonly found process in the polygenetic environment of the Himalayas (Benn and Owen 2002). The field-based geomorphologic study by Barnard *et al.* (2004) has been confirmed that upper Bhagirathi valley is very sensitive to post-depositional sedimentation by mass movement and glacio-fluvial processes on lateral slopes of mountain terrain.

Temperatures of debris-covered ice, snow, clean ice and surrounding moraine materials vary greatly due to their internal structure and chemical properties (Mihalcea *et al.* 2006, 2007; Suzuki *et al.* 2007). However, cold debris and sand nears the glacier snout has been miss-classified as debris-covered glacier during the mapping from thermal data (Shukla *et. al.* 2010). We also recognize similar results using ASTER and ETM+ thermal data. This misclassified information can be corrected using geomorphometric parameters. The different slope values are helpful in segregating the tributary hanging glacier from main valley glacier. Morphometric parameters such as slope, plan and profile curvatures derived from the ASTER DEM allows the mapping of debris-

covered glaciers. Profile curvature enables the lateral moraines to be identified whereas plan curvature allows the differentiating of the glacier front to the almost flat valley floor of the direct glacier forefield. Previous studies have recognized great potential of plan and profile curvature for identifying the margins of the snouts of valley glaciers (Bishop *et al.* 2001, Bolch and Kamp 2006, Bolch *et al.* 2007).

We notice that during the selection of threshold for single thermal band of ASTER is a crucial step. Increase or decrease of the threshold value of 0.1 influences significantly the enlargement or reduction of glacier area and its surrounding coverage.

The results from clean ice glacier mapping based on ASTER band 3 and 4 also covered dark shadow areas and some rocky areas within the glacier. For accurate mapping of clean glacier area, it is essential to further improve these misclassifications, e.g. with using the blue wavelength (Paul and Kääb, 2005) and manual improvements However it is possible to successfully distinguish the transition between debris-covered ice and clean glacier ice.

It appears that shadow areas strongly affect the single thermal band thresholding which can hamper the automatic mapping of debris-covered areas. Thresholding procedure of satellite images is scene-dependant and subjective in nature (depends on the interpreter). Visually detection of debris-covered ice may be strongly enhanced by utilizing stereo-viewing techniques on the stereo images e.g. using ASTER bands 3N and 3B (Racoviteanu *et al.* 2009).

The present methodology with an uncertainty of about 5% is promising for the mapping and monitoring of other large debris-covered glaciers such as Bada Shigri Glacier (Himachal Himalayas). This approach can further ameliorate using high resolution DEMs derived from high resolution data such as Cartosat or TanDEM-X and high-resolution multi-spectral data. However, currently only Landsat ETM+ thermal band has higher spatial resolution as compared to other satellite programs. Therefore there is a need to improve the thermal sensor spatial resolution

Conclusions

1 The results from mapping the debris-covered Gangotri Glacier confirm the strong potential of the presented approach based on the ASTER DEM and thermal data from its unique large cave at the snout and its orientation from southeast to northwest in the years 2001 and 2006.

2 Chorabari Glacier could not be mapped semi-automatically with suitable accuracy due to its complex end moraine near its snout area. The ASTER DEM could not perceive this polygenetic landscape complication, which could stem from the resolution of ASTER data. This indicates that resolution of ASTER stereo data and thermal band is inadequate for mapping smaller debris-covered glaciers in the Garhwal Himalayas.

3 The high resolution Cartosat-I image was helpful for the interpretation of polygenetic complex mountainous landscape. The problematic areas that were not mapped by presented approach were closely associated with resolution of ASTER data (figure 9).

4 The post-depositional sedimentation by debris flow/mass movement was appeared a great hindrance for the automated mapping of debris-covered glaciers in the polygenetic environment of the Himalayas. The shadow areas strongly affect the single thermal band thresholding which can hamper the automatic mapping of debris-covered areas. Thresholding procedure is scene-dependant and subjective in nature (depends on the interpreter).

5 Thresholding of slope has a great potentiality to map those debris-covered glacier snouts. However, the thresholds have to be carefully selected.

6 The semi-automated debris-covered mapping approach presented in this paper could be extended to larger debris-covered glaciers in the Himalayas and other mountain regions. However, care must be taken during the selection of thresholds and cluster groups due to regional setting of relief, quantity of debris load, orientation, and climatic conditions vary considerably throughout the Himalayas and other mountains regions and even within one basin.

1

2

Acknowledgments

3 The Director, Wadia Institute of Himalayan Geology, Dehradun is thankfully acknowledged for his
4 support for the present work. The first author is grateful to S.C. Kulshreshtha (Reader, SD College,
5 Muzaffarnagar) for valuable guidance and support. Thanks are also due to Kanhaiya Singh (Survey
6 Expert, Project Activity Core Team, UPWSRP, Lucknow). S.K. Goyal (Principal, GNKC, Karnal)
7 and Pushpinder Kaur (GNKC) for their wholehearted support. The authors also express their
8 appreciation to Prashant Kawishwar, Resource Scientist, Department of Science and Technology,
9 Chattisgarh for thoughtful discussion on glacier mapping. We are also grateful to Lokesh Sharma
10 (Librarian, Ratan Tata Library, Delhi University) for providing valuable references. The authors
11 extend their gratitude to two anonymous reviewers whose insightful comments and suggestions
12 greatly improved the manuscript. Further thanks are directed to Susan Braun-Clarke who polished
13 the English. This article benefited from the results of the project "Monitoring of glaciers and glacial
14 lakes at Mt. Everest/Nepal based on ASTER data" founded by the German Research Foundation
15 (Deutsche Forschungsgemeinschaft, DFG) under the code BU 949/15-1. ASTER data was provided
16 at no cost by NASA/USGS under the umbrella of the GLIMS project.

17

18

19

20

21

References

22 ACKERMAN, T., ERICKSON, T. and WILLIAMS, M.W., 2001, Combining GIS and GPS to
23 Improve Our Understanding of the Spatial Distribution of Snow Water Equivalence (SWE).
24 Talk presented by T. Erickson at the 2001 ESRI Users Conference. San Diego, California,

on July 10, 2001, http://snobear.colorado.edu/Markw/Research/ESRI/ESRI.html accessed on 15th February, 2009.

AHMAD, S. and HASNAIN, S. I., 2004, Analysis of satellite imageries for characterization of glacio-morphological features of the Gangotri Glacier, Ganga headwater, Garhwal Himalayas. In Proceedings: Workshop on Gangotri Glacier, D. Srivastava, K.R. Gupta. & . S. Mukerji (Ed.), *Geological Survey of India,* **80**, pp. 61-67.

ALBERT, T.H., 2002, Evaluation of remote sensing techniques for ice-area classification applied to the tropical Quelccaya ice cap, Peru. *Polar Geography,* **26**, pp. 210–226.

ANDREASSEN, L. M., PAUL, F., KAAB, A. and HAUSBERG, J. E., 2008, The new Landsat-derived glacier inventory for Jotunheimen, Norway, and deduced glacier changes since the 1930s. *The Cryosphere,* **2**, pp. 131-145.

BAHUGUNA, I.M., 2008, Himalayan Glaciers. *ISG Newsletter.* **14**, pp. 36-43.

BAHUGUNA, I.M., RATHORE, B. P., NEGI, H. S., KULKARNI, A. V., and MATHUR, P., 2004, Fusion of panchromatic and multi-spectral Indian Remote Sensing satellite images for identification of Gangotri Glacier snout. In Proceedings: Workshop on Gangotri Glacier, D. Srivastava, K.R. Gupta. & . S. Mukerji (Ed.), *Geological Survey of India,* **80**, pp. 61-67.

BARNARD, P. L., OWEN, L. A. and FINKEL, R. C., 2004, Style and timing of glacial and paraglacial sedimentation in a monsoon-influenced high Himalayan environment, the upper Bhagirathi Valley, Garhwal Himalaya. *Sedimentary Geology*, pp. 199–221.

BENN, D. I. and EVANS, D.J.A., 1998, Glaciers and glaciation, pp. 734 (New York, Arnold).

BENN, D. I. and OWEN, L. A., 2002, Himalayan glacial sedimentary environments: A framework for reconstructing and dating the former extent of glaciers in high mountains. *Quaternary International,* **97**, pp. 3–25.

BENN, D.I, WISEMAN, S and WARREN, C.R., 2000, Rapid growth of supraglacial lake, Ngozumpa Glacier, Khumbu Himal, Nepal: *IAHS-AISH Publication,* **264**. pp. 177-185.

BERTHIER, E., ARNAUD, Y., KUMAR, R., AHMAD, S., WAGNON, P. and CHEVALLIER, P., 2007, Remote sensing estimates of glacier mass balances in the Himachal Pradesh (Western Himalayas, India). *Remote Sensing of Environment,* **108**, pp. 327−338.

BHAMBRI**,** R**.** and BOLCH, T., 2009, Glacier Mapping: A Review with special Reference to the Indian Himalayas. *Progress in Physical Geography*, **33**, pp. 672–704.

BISHOP, M. P., BONK, R., KAMP, U. and SHRODER, Jr., J. F., 2001, Terrain analysis and data modeling for alpine glacier mapping. *Polar Geography,* **25**, pp.182– 201.

BISHOP, M. P., SHRODER, Jr., J. F. and HICKMAN. B.L., 1999, SPOT panchromatic imagery and neural networks for information extraction in a complex mountain environment. *Geocarto International*, **14,** pp.19–28.

BISHOP, M. P., SHRODER, Jr., J. F. and WARD. J.L., 1995, SPOT Multispectral analysis for producing supraglacial debris-load estimates for Batura Glacier, Pakistan. *Geocarto International*, **10**, pp.81–90**.**

BOLCH, T., BUCHROITHNER, M. F., KUNERT, A. and KAMP, U., 2007, Automated delineation of debris-covered glaciers based on ASTER data. In *GeoInformation in Europe*, M. A. Gomarasca (Ed.), pp. 403–410 Millpress, Netherlands.

BOLCH, T., BUCHROITHNER, M. F., PETERS, J., BÄßLER, M. and BAJRACHARJA, S., 2008b, Identification of glacier motion patterns and potential dangerous glacial lakes at Mt. Everest using space imagery. *Natural Hazards and Earth System Sciences,* **8**, pp.1329-1340.

BOLCH, T., BUCHROITHNER, M. F., PIECZONKA, T. and KUNERT, A., 2008a, Planimetric and volumetric Glacier changes in Khumbu Himalayas since 1962 using Corona, Landsat TM and ASTER data. *Journal of Glaciology*, pp. 592-600.

BOLCH, T. and KAMP, U., 2006, Glacier mapping in high mountains using DEMs, Landsat and ASTER data. *Grazer Schriften der Geographie und Raumforschung*, 41 (=*Proc.8th Int.*

Symp. on High Mountain Remote Sensing Cartography, 20.-27.3.2005, La Paz, Bolivia), pp 37−48.

BOLCH, T., MENOUNOS, B., WHEATE, R., 2010, Landsat-based glacier inventory of western Canada, 1985-2005. *Remote Sensing of Environment* 114, pp. 127-137. doi:10.1016/j.rse.2009.08.015.

BRENNING, A., 2009. Benchmarking classifiers to optimally integrate terrain analysis and multispectral remote sensing in automatic rock glacier detection. *Remote sensing of environment*. **113**, pp. 239-247.

CHAUJAR, R. K., MAZARI, R. K and GERGAN, J. T., Glacial geomorphology of the Gaumukh – the source of Ganga, with referance to its present state of environment. Seminar on Ganga in the Service of the Nation, University of Roorkee, 12–13 September 1993, II1–II14.

CONRAD, O., 2006, SAGA - program structure and current state of implementation. In SAGA - Analysis and Modelling Applications. pp 39-52, 2006 Böhner, J., McCloy K.R. and Strobl, J. (Eds.), *Göttinger Geographische Abhandlungen*,

DOBHAL, D.P. and Kumar, S., 1996, Inventory of glacier basins in Himachal Himalayas. *Journal of Geological Society of India*, pp 671-681.

FISCHER, L., KÄÄB, A., HUGGEL, C. and NOETZLI, J., 2006. Geology, glacier retreat and permafrost degradation as controlling factors of slope instabilities in a high-mountain rock wall: the Monte Rosa east face. *Natural Hazards and Earth System Sciences*, **6**, pp.761 - 772.

FORGY, E., 1965, Cluster analysis of multivariate data: Efficiency vs. interpretability of classifications. *Biometrics*, **21**, pp. 768.

FORT, M., 2000, Glaciers and mass wasting processes: their influence on the shaping of Kali Gandaki valley, Nepal. *Quaternary International,* **65**, pp. 101–119.

FUSHIMI, H., YOSHIDA, M., WATANABE, O. and UPADHYAY, B.P., 1980, Distributions and grain sizes of supraglacial debris in the Khumbu Glacier, Khumbu Region, East Nepal. In: Glaicers and Climates of Nepal Himalayas. Report of the Glaciological Expedition to Nepal: Part 4. *Seppyo*, Higuchi, K., Hakajima, C. and Kusunoki, K., (Eds.) **41** , pp. 18-25.

GRANSHAW, F.D. and A.G. FOUNTAIN. 2006. Glacier change (1958– 1998) in the North Cascades National Park Complex, Washington, USA. *Journal of Glaciology.* **52**, pp.251–256.

HAMBREY, M., QUINCEY, D., GLASSER, N. F. and REYNOLDS, J. M., 2008, Sedimentological, geomorphological and dynamic context of debris-mantled glaciers, Mount Everest (Sagarmatha) region, Nepal. *Quaternary Science Reviews,* **27,** 2341-2360.

HEWITT, K., 2009, Rock avalanches that travel onto glaciers and related developments, Karakoram Himalaya, Inner Asia. *Geomorphology,* **103**, pp. 66–79.

IMMERZEEL, W. W., VAN BEEK, L. P. H. and BIERKENS, M. F. P., 2010. Climate change will affect the Asian water towers, *Science*, **328**, pp. 1382-1385.

IWATA, S., TATSUTO, A., TSUTOMU, K., KATSUMOTO, S. and SATORU, Y., 2000. Morphological evolution of the debris cover on Khumbu Glacier, Nepal, between 1978 and 1995. IAHS Publication no. **264,** pp.3-11.

KÄÄB, A., 2002, Monitoring high mountain terrain deformation from repeated air- and spaceborne optical data: examples using digital aerial imagery and ASTER data, *ISPRS-Journal of. Photogrammetry and Remote Sensing*, **57**, pp. 39–52.

KÄÄB, A., HUGGEL, C. and FISCHER, L., 2006, Remote sensing technologies for monitoring climate change impacts on glacier- and permafrost-related hazards. *2006 ECI Conference on Geohazards.* Paper **2**, pp. 12.

KAMP, U., BOLCH, T. and OLSENHOLLER J., 2005. Geomorphometry of Cerro Sillajhuay, Chile/Bolivia: comparison of DEMs derived from ASTER remote sensing data and contour maps. *Geocarto International,* **20**, pp. 23-34.

KARGEL, J., ABRAMS, M., BISHOP, M., BUSH, A., HAMILTON, G. and JISKOOT, H., 2005, Multispectral imaging contributions to global land ice measurements from space. *Remote Sensing of Environment,* **99**, pp.187−219.

KELLERER-PIRKLBAUER, A., 2008. The Supraglacial Debris System at the Pasterze Glacier, Austria: Spatial Distribution, Characteristics and Transport of Debris. Z. *Geomorph. N.F.* **52**, pp.3-25.

KESHRI, A. K., SHUKLA, A. and GUPTA, R. P., 2009, ASTER ratio indices for supraglacial terrain mapping. *International Journal of Remote Sensing*, **30**, pp. 519 – 524.

KIRKBRIDE, M.P., 1995. Processes of transportation. In *Modern glacial environments: processes, dynamics and sediments. Vol. 1.* Glacial environments J. Menzies Ed. pp. 261–292. Butterworth- Heinemann: Oxford

KOMORI, J., 2008, Recent expansions of glacial lakes in the Bhutan Himalayas. *Quaternary International,* **184**, pp. 177- 186.

KULKARNI, A. V., BAHUGUNA, I.M., RATHORE, B. P., SINGH, S.K., RANDHAWA, S.S., SOOD, R.K. and DHAR, S. 2007, Glacial retreat in Himalayas using Indian Remote Sensing satellite data. *Current Science,* **92**, pp. 69-74.

KULKARNI, A. V., RATHORE, B. P., MAHAJAN, S. and MATHUR, P. 2005, Alarming retreat of Parbati glacier, Beas basin, Himachal Pradesh, *Current Science,* **88**, pp. 1844-1849.

KULKARNI, A. V. and SUJA, A.M., 2003, Estimation of recent glacial variations in Baspa Basin using remote sensing techniques. *Journal of Indian Society of Remote Sensing,* **31**, pp. 81–90.

MATTSON, L. E., 2000, The influence of a debris cover on the mid-summer discharge of Dom Glacier, Canadian Rocky Mountains: *IAHS-AISH Publication.* **264**, pp. 25-33.

MIHALCEA, C., BROCK, B.W., DIOLAIUTI, G., D'AGATA, C., CITTERIO, M., KIRKBRIDE, M.P., CUTLER, M.E.J. and SMIRAGLIA, C., 2007, Using ASTER satellite and ground-based temperature measurements to derive supraglacial debris cover and thickness patterns on Miage Glacier (Mont Blanc massif, Italy). Cold Regions Science and Technology doi: 10.1016/j.coldregions.2007.3.004

MIHALCEA, C., MAYER, C., DIOLAIUTI, G., LAMBRECHT, A., SMIRAGLIA, C. and TARTARI, G., 2006, Ice ablation and meteorological conditions on the debriscovered area of Baltoro Glacier (Karakoram, Pakistan). *Annals of Glaciology*, **43**, pp. 292–300.

NAITHANI, A.K., NAINWAL, H.C., SATI, K.K. and PRASAD, C., 2001, Geomorphological evidences of retreat of the Gangotri glacier and its characteristics. *Current Science,* **80**, pp. 87-94.

PAUL, F., BARRY, R., COGLEY, J.G., FREY, H., HAEBERLI, W., OHMURA, A., OMMANNEY, S., RAUP, B., RIVERA, A. and ZEMP, M., 2009, Recommendations for the compilation of glacier inventory data from digital sources. *Annals of Glaciology*, **50**, pp.119-126

PAUL, F., HUGGEL, C. and KÄÄB, A., 2004, Mapping of debris-covered glaciers using multispectral and DEM classifcation techniques. *Remote Sensing of Environment,* **89**, pp. 510-518.

PAUL, F., KÄÄB, A., MAISCH, M., KELLENBERGER, T. and HAEBERLI, W., 2002, The new remote sensing derived Swiss glacier inventory: I Methods. *Annals of Glaciology,* **34**, pp. 355-361.

PELTO, M. S., 2000, Mass balance of adjacent debris-covered and clean glacier ice in the North Cascades, Washington: *IAHS-AISH Publication,* **264**, pp. 35-42.

PHILIP, G. and RAVINDRAN, K.V., 1998, Glacial mapping using Landsat Thematic mapper data: a case study in parts of Gangotri glacier, NW Himalayas. *Indian Journal of Remote Sensing,* **26**, pp. 29–34.

POPOVNIN, V.V. and ROZOVA. A. 2002. Influence of sub-debris thawing on ablation and runoff of the Djankuat Glacier in the Caucasus. *Nordic Hydrology*, **33,** pp.75–94.

QUINCEY, D.J., LUCAS, R.M., RICHARDSON, S.D., GLASSER, N.F., HAMBREY, M.J. and REYNOLDS, J.M., 2005, Optical remote sensing techniques in high-mountain environments: application to glacial hazards. *Progress in Physical Geography*, **29,** pp.475-505.

RACOVITEANU, A.E., ARNAUD, Y., WILLIAMS, M., and ORDONEZ, J., 2008, Decadal changes in glacier parameters in the Cordillera Blanca, Peru, derived from remote sensing. *Journal of Glaciology*, **54**, pp. 499-510.

RACOVITEANU, A.E., MANLEY, W.F., ARNAUD, Y. and WILLIAMS, M., 2007, Evaluating digital elevation models for glaciologic applications: An example from Nevado Coropuna, Peruvian Andes. *Global Planet Change,* **59**, pp. 110-125.

RACOVITEANU, A.E., PAUL, F., RAUP, B., KHALSA, S.J.S. and ARMSTRONG, R., 2009, Challenges and recommendations in mapping of glacier parameters from space: results of the 2008 Global Land and Ice Measurements from Space (GLIMS) workshop, Boulder, Colorado, USA. *Annals of Glaciology,* **50**, pp. 53-69.

RANZI, R., GROSSI, G., IACOVELLI, L., and TASCHNER, T., 2004, Use of Multispectral ASTER images for mapping debris-covered glaciers within the GLIMS Project. *IEEE International Geoscience and Remote Sensing Symposium.* pp. 1144-1147.

RAUP, B.H., KÄÄB, A., KARGEL, J.S., BISHOP, M.P., HAMILTON, G., LEE, E., PAUL, F., RAU, F., SOLTESZ, D., KHALSA, S.J.S., BEEDLE, M., and HELM, C., 2007, Remote

Sensing and GIS Technology in the Global Land Ice Measurements from Space (GLIMS) Project. *Computers and Geosciences*, **33**, pp. 104-125.

REYNOLDS, J.M., 2000. On the formation of supraglacial lakes on debris-covered glaciers: *IAHS-AISH Publication*. **264**, pp. 153–161.

SCHMIDT, S. and NÜSSER, M., 2009. Fluctuations of Raikot Glacier during the past 70 years: a case study from the Nanga Parbat massif, northern Pakistan. **55**, pp. 949–959.

SHRODER, J.F., JR., BISHOP, M.P., SLOAN, V. and COPLAND, L., 2000, Debris-covered glaciers and rock glaciers in the Nanga Parbat Himalayas, Pakistan. *Geografiska Annaler*, pp.17-31.

SHUKLA, A. GUPTA, R.P. and ARORA, M.K., 2009, Estimation of debris cover and its temporal variation using optical satellite sensor data: a case study in Chenab basin, Himalaya. *Journal of Glaciology*. **55**, pp. 444–452.

SHUKLA, A. ARORA, M.K and GUPTA R.P., 2010. Synergistic approach for mapping debris-covered glaciers using optical-thermal remote sensing data with inputs from geomorphometric parameters, *Remote Sensing of Environment*, **114**, pp. 1378-1387.

SIDJAK, R. and WHEATE, R., 1999, Glacier mapping of the Illecillewaet icefield, British Columbia, Canada, using Landsat TM and digital elevation data. *International Journal of Remote Sensing,* **20**, pp. 273–284.

SMALL, RJ. 1987. Englacial and supraglacial sediment transport and deposition. In Glacio-fluvial Sediment Transfer; An Alpine Perspective, Gurnell AM, Clark MJ (Ed.), pp. 111–145. (Chichester: John Wiley & Sons).

STOKES, C.R., POPOVNIN, V., ALEYNIKOV, A., GURNEY, S.D. and SHAHGEDANOVA, M. 2007. Recent glacier retreat in the Caucasus Mountains, Russia, and associated increase in supraglacial debris cover and supra/proglacial lake development. *Annals of Glaciology*.**46**, pp.195-203.

SUZUKI, R., FUJITA, K., and AGETA, Y., 2007. Spatial distribution of thermal properties on debris-covered glaciers in the Himalayas derived from ASTER data. *Bulletin of Glaciological Research*, **24**, pp.13–22.

TOUTIN, T. 2004. Review article: Geometric processing of remote sensing images: models, algorithms and methods. *International Journal of Remote Sensing*, **25**, pp.1893 – 1924.

TOUTIN, T. 2008. ASTER DEMs for geomatic and geoscientific applications: a review. *International Journal of Remote Sensing*, **29**, pp. 1855-1875.

TASCHNER, S., and RANZI, R. 2002. Comparing opportunities of Landsat-TM and ASTER data for monitoring a debris-covered glacier in the Italian Alps within the GLIMS project. IEEE transactions on geoscience and remote sensing symposium, June (pp. 24−28).

ZEVENBERG, L. W. and C. R. THORNE 1987, Quantitative analysis of land surface topography. Earth Surface Processes and Landforms, **12**, pp. 47-56.

Figures captions

Figure 1 ASTER 3-3-1 band image (2006) overlaid on the ASTER DEM.

Figure 2(*a*) Snout of Gangotri Glacier, (*b*) Supra-glacial lake in ablation zone of Gangotri Glacier, (*c*) Crevasse in ablation zone of Gangotri Glacier, (*d*) Closer view of crevasse in ablation zone of Gangotri Glacier (Source: Bhambri and Chaujar-2007).

Figure 3(*a*) End moraine of Chorabari Glacier and, (*b*) Debris-covered ablation area of Chorabari Glacier (Source: Bhambri and Chaujar, 2006).

Figure 4(*a and a''*) Unnatural peaks in accumulation zone of hill shaded ASTER DEM, (*b*) Removal of unnatural peaks in hill shaded ASTER DEM.

Figure 5 Scheme for automated mapping of debris-covered glaciers.

Figure 6(*a*) FCC image of ASTER image, (*b*) Cluster analysis of plan and profile curvature in ten categories, (*c*) Reclustering of plan, profile curvature and slope in ten classes, (*d*) Re-clustering of plan, profile curvature and slope in three categories, (*e*) Vectorization of three classes, 6(*f*) Selected Gangotri Glacier vector layer overlaid on ASTER FCC.

Figure 7(*a*) Thermal band 12 of ASTER image, (*b*) Thermal mask for debris-covered area in binary format, (*c*) Vectorization of thermal mask, (*d*) Selected thermal mask vector layer overlaid on thermal band.

Figure 8(*a*) Band ratio image of ASTER data based on bands 3 and 4, (*b*) Vector layer derived from band ratio overlaid on ASTER FCC.

Figure 9 Comparison between automated and manually digitized outlines of the Gangotri Glacier.

Figure 10 Reclassified cluster analysis in pink color based on (*a*) 2001 and (*b*) 2006 ASTER DEM overlaid on ASTER Image.

Figure 11(*a*) Cartosat-I image, (*b*) Vector layer derived from reclassified cluster analysis overlaid on Cartosat-I image.

Figure 12 Average optimum slope calculations from ASTER DEM for Gangotri glacier (*a*) FCC of ASTER image, (*b*) 15 degree slope (light green colour), (*c*) 18 degree slope (orange colour), (*d*) 25 degree slope (dark green colour).

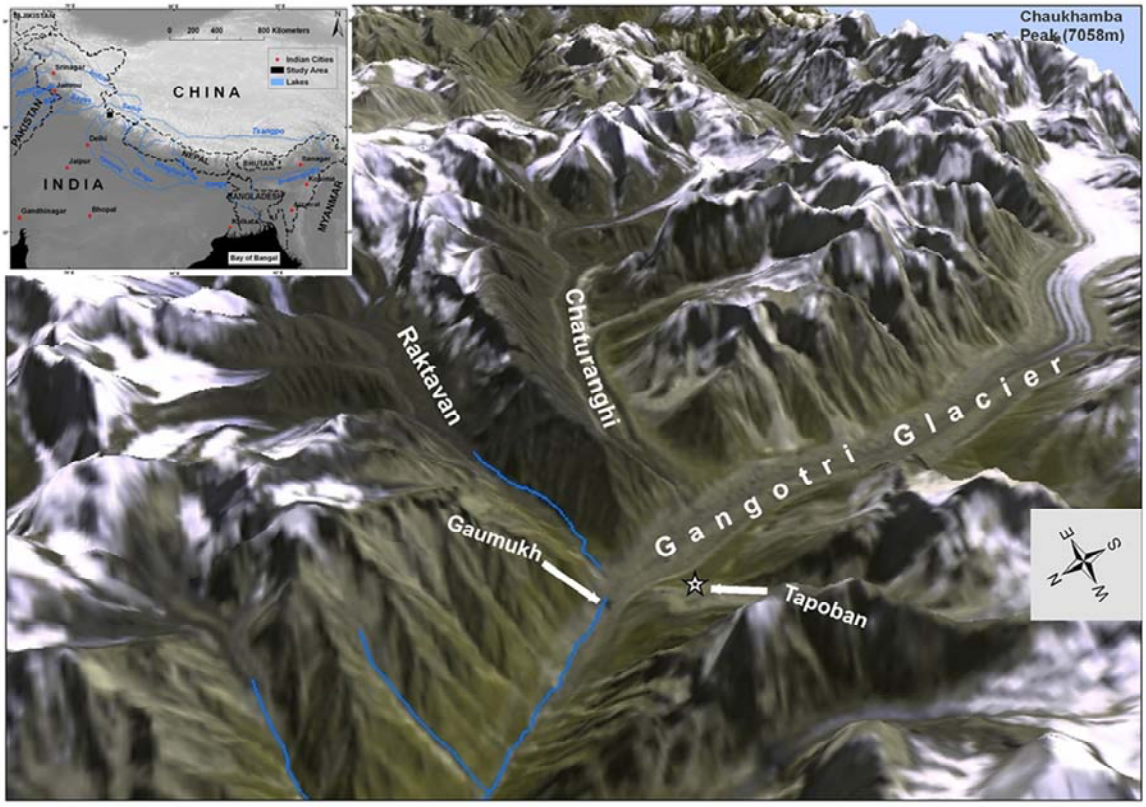

Figure 1 ASTER 3-3-1 band image (2006) overlaid on the ASTER DEM.

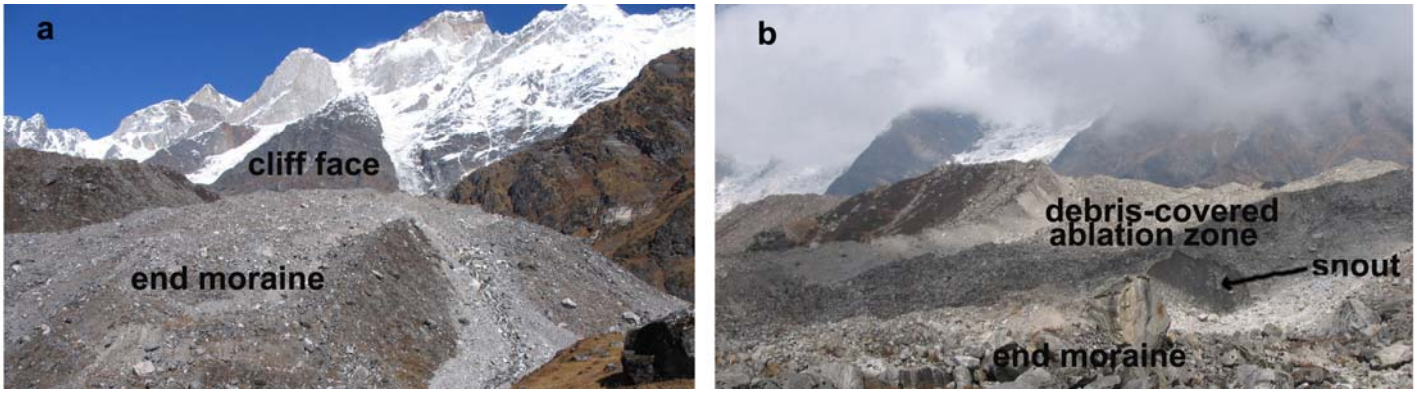

Figure 2(*a*) End moraine of Chaurabari Glacier and, (*b*) Debris-covered ablation area of Chaurabari Glacier (Source: Bhambri and Chaujar, 2006).

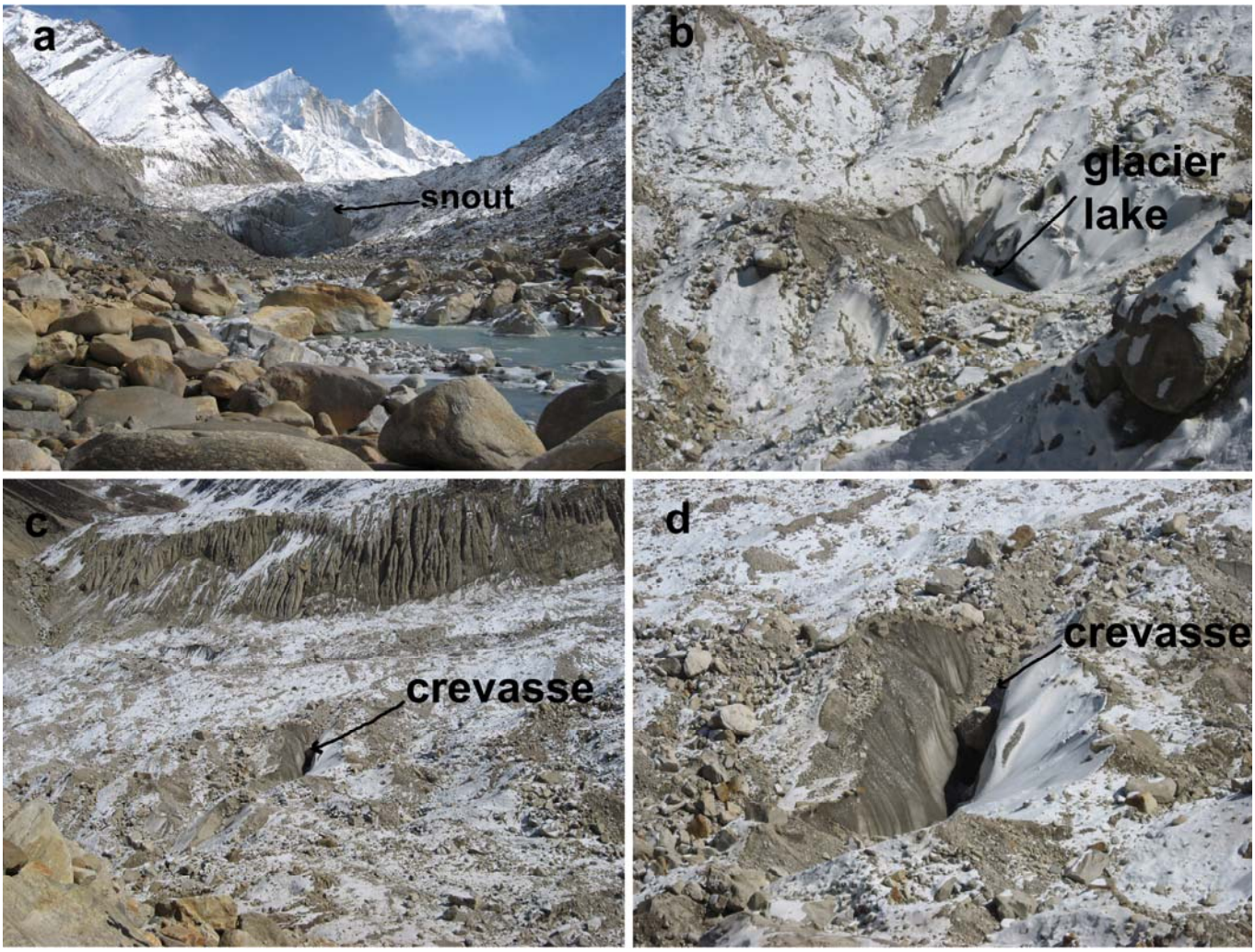

Figure 3(*a*) Snout of Gangotri Glacier, (*b*) Supra-glacial lake in ablation zone of Gangotri Glacier, (*c*) Crevasses in ablation zone of Gangotri Glacier, (*d*) Closer view of crevasses in ablation zone of Gangotri Glacier (Source: Bhambri and Chaujar-2007).

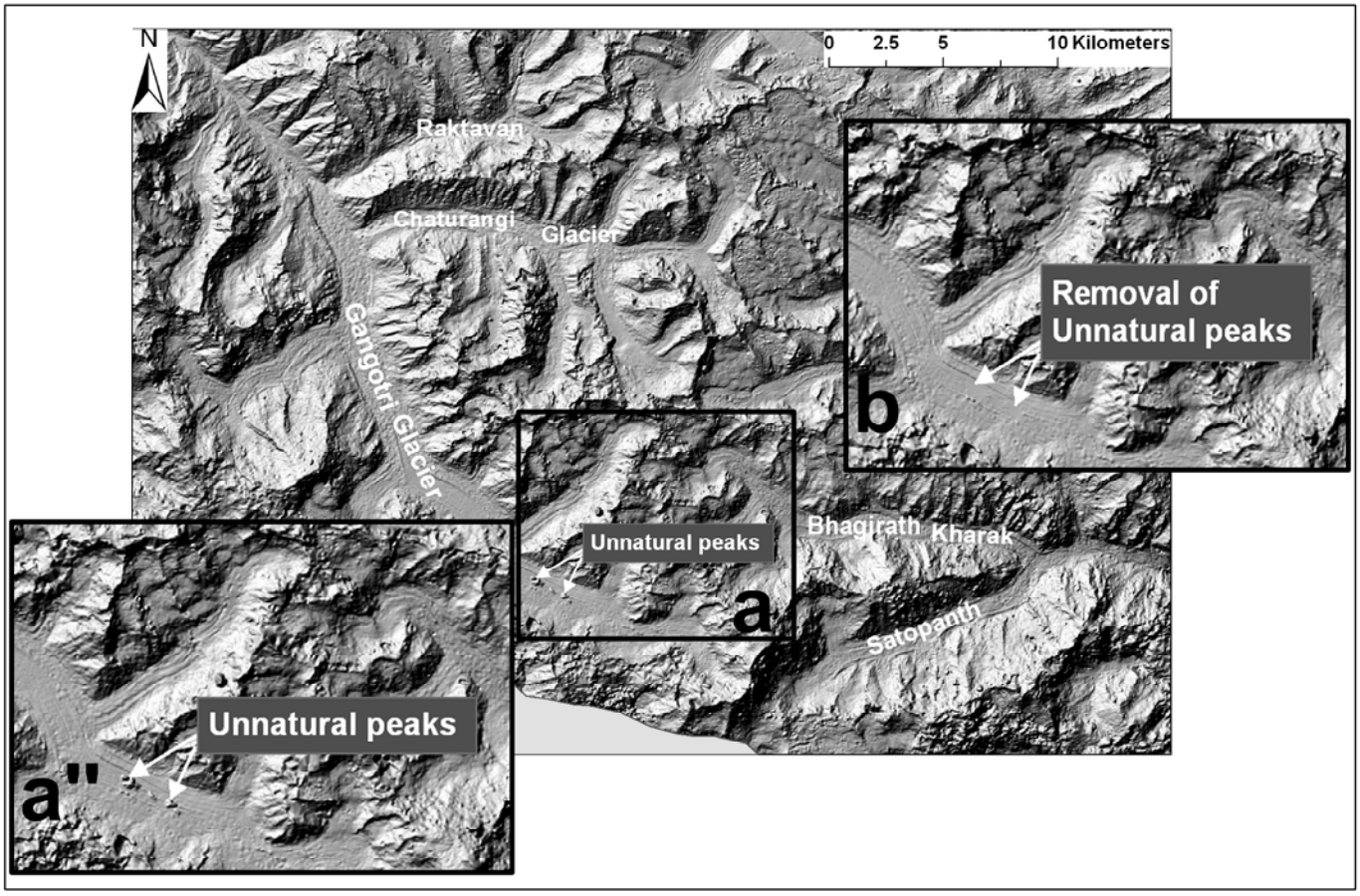

Figure 4(*a and a''*) Unnatural peaks in accumulation zone of hill shaded ASTER DEM, (*b*) Removal of unnatural peaks in hill shaded ASTER DEM.

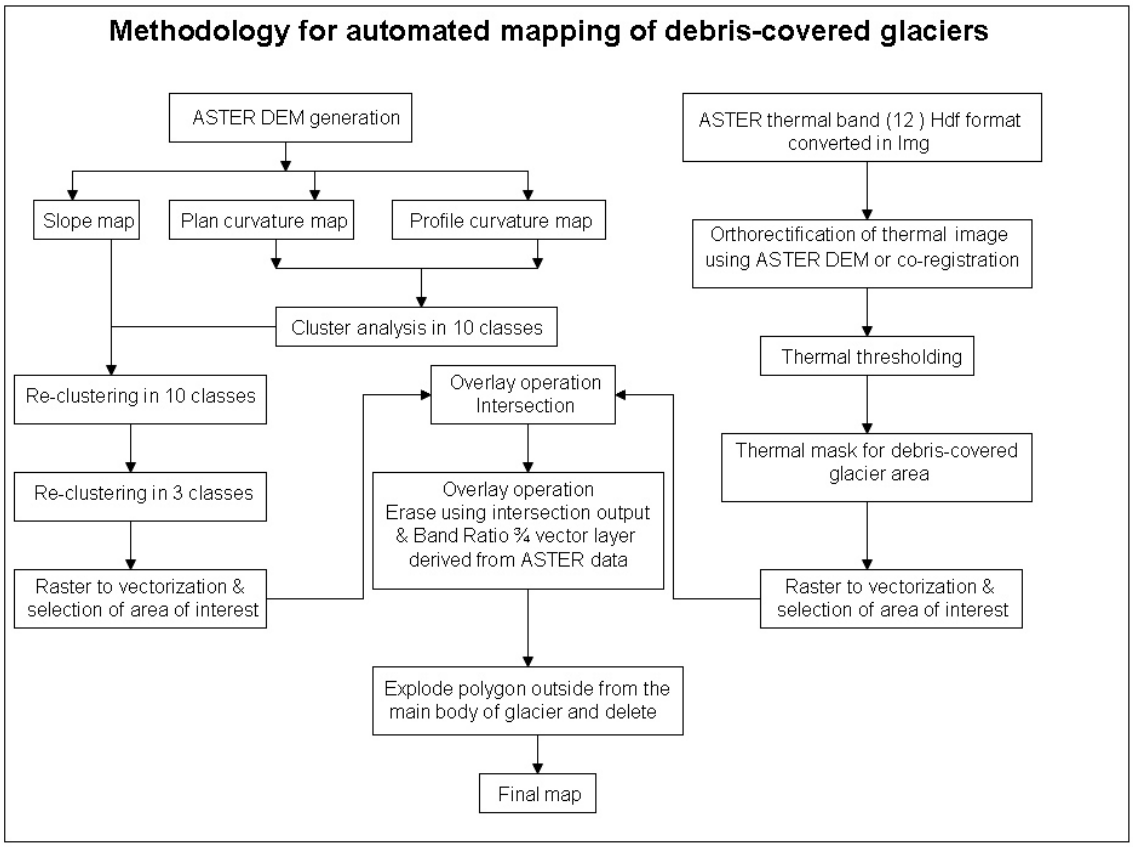

Figure 5 Scheme for automated mapping of debris-covered glaciers.

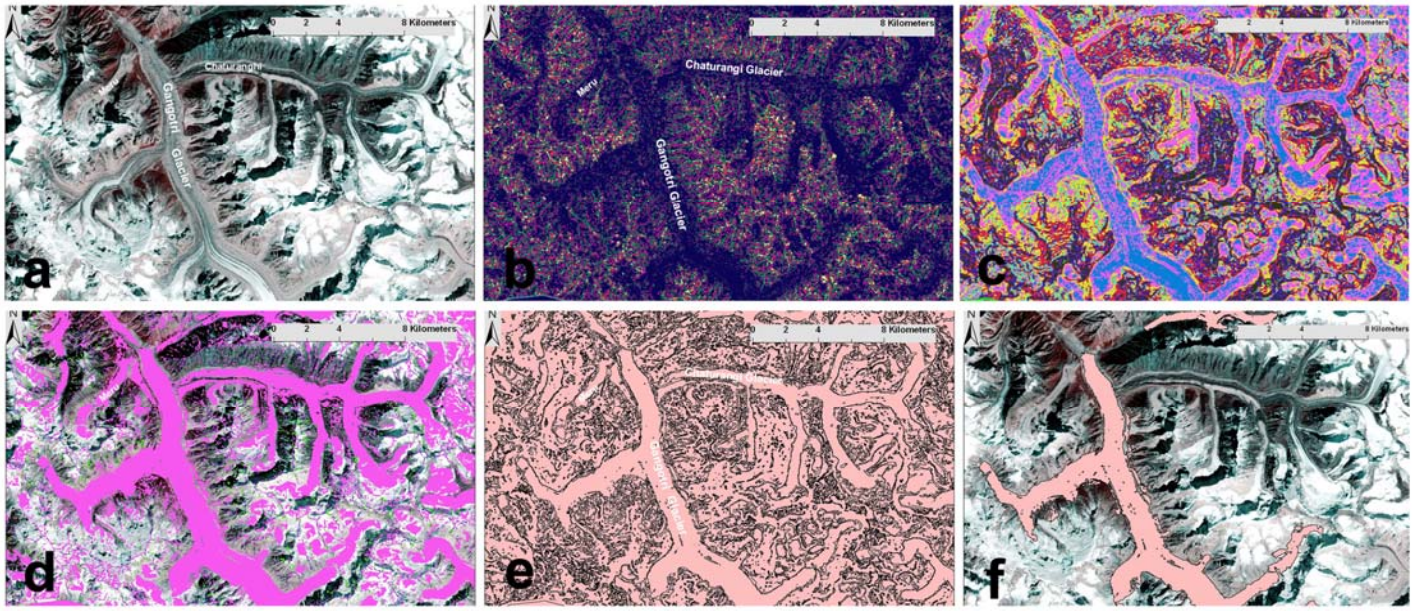

Figure 6(*a*) FCC image of ASTER image, (*b*) Cluster analysis of plan and profile curvature in ten categories, (*c*) Reclustering of plan, profile curvature and slope in ten classes, (*d*) Re-clustering of plan, profile curvature and slope in three categories, (*e*) Vectorization of three classes, (*f*) Selected Gangotri Glacier vector layer overlaid on ASTER FCC.

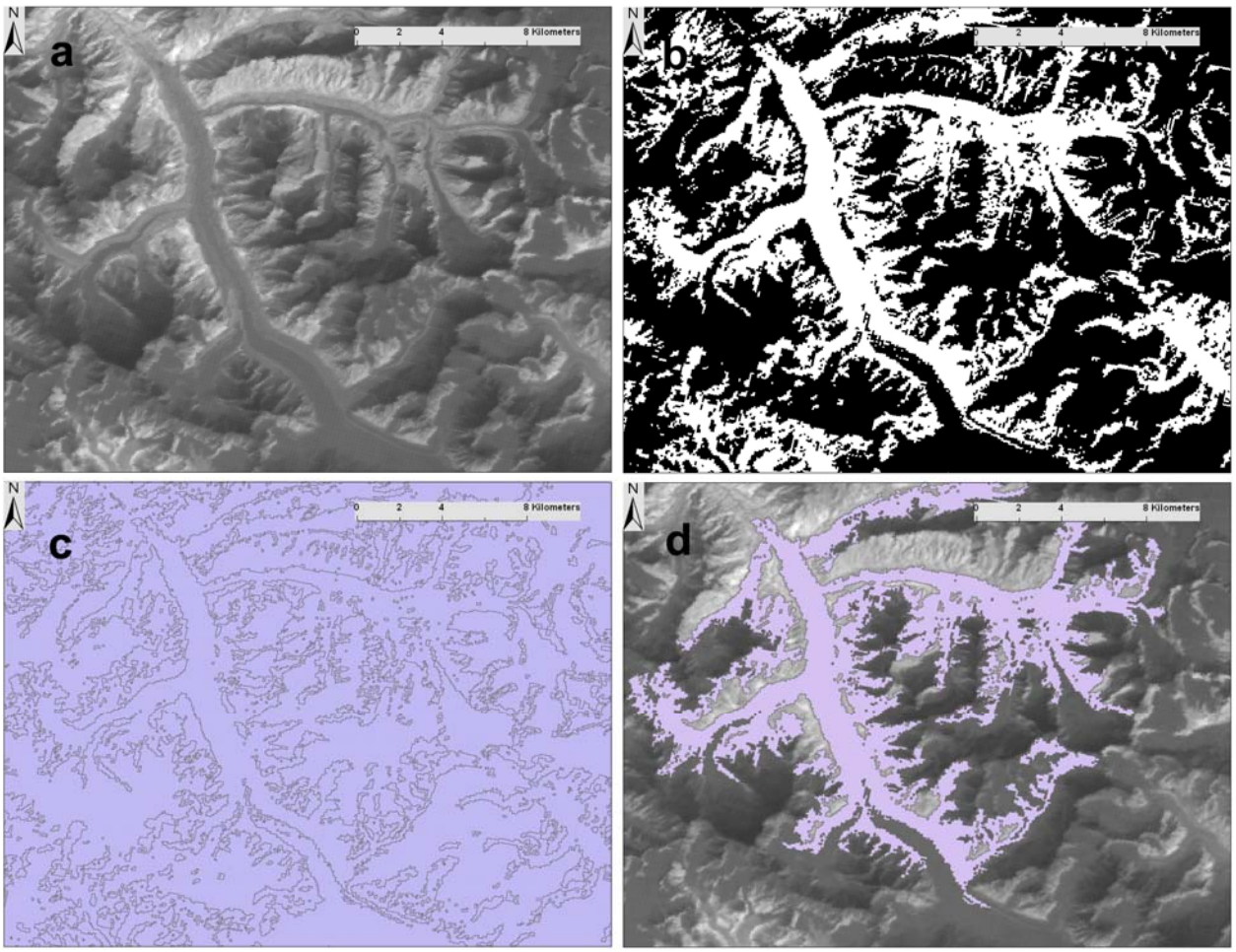

Figure 7(*a*) Thermal band 12 of ASTER image, (*b*) Thermal mask for debris-covered area in binary format, (*c*) Vectorization of thermal mask, (*d*) Selected thermal mask vector layer overlaid on thermal band.

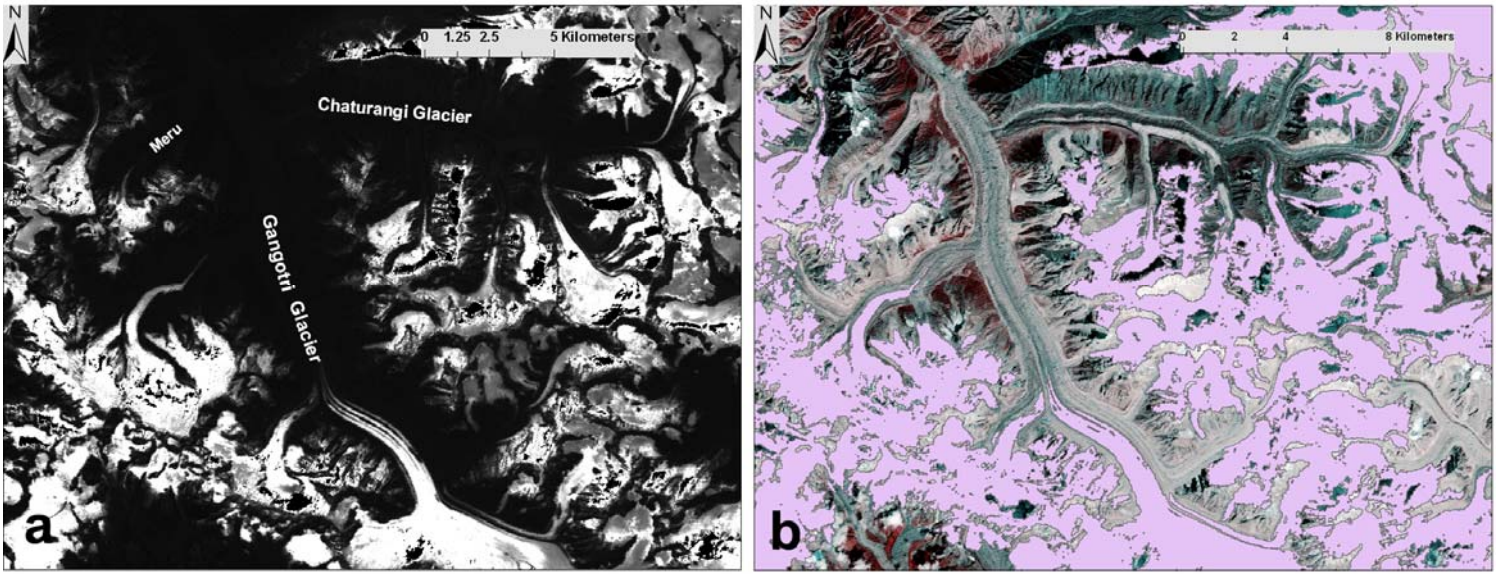

Figure 8(*a*) Band ratio image of ASTER data based on bands 3 and 4, (*b*) Vector layer derived from band ratio overlaid on ASTER FCC.

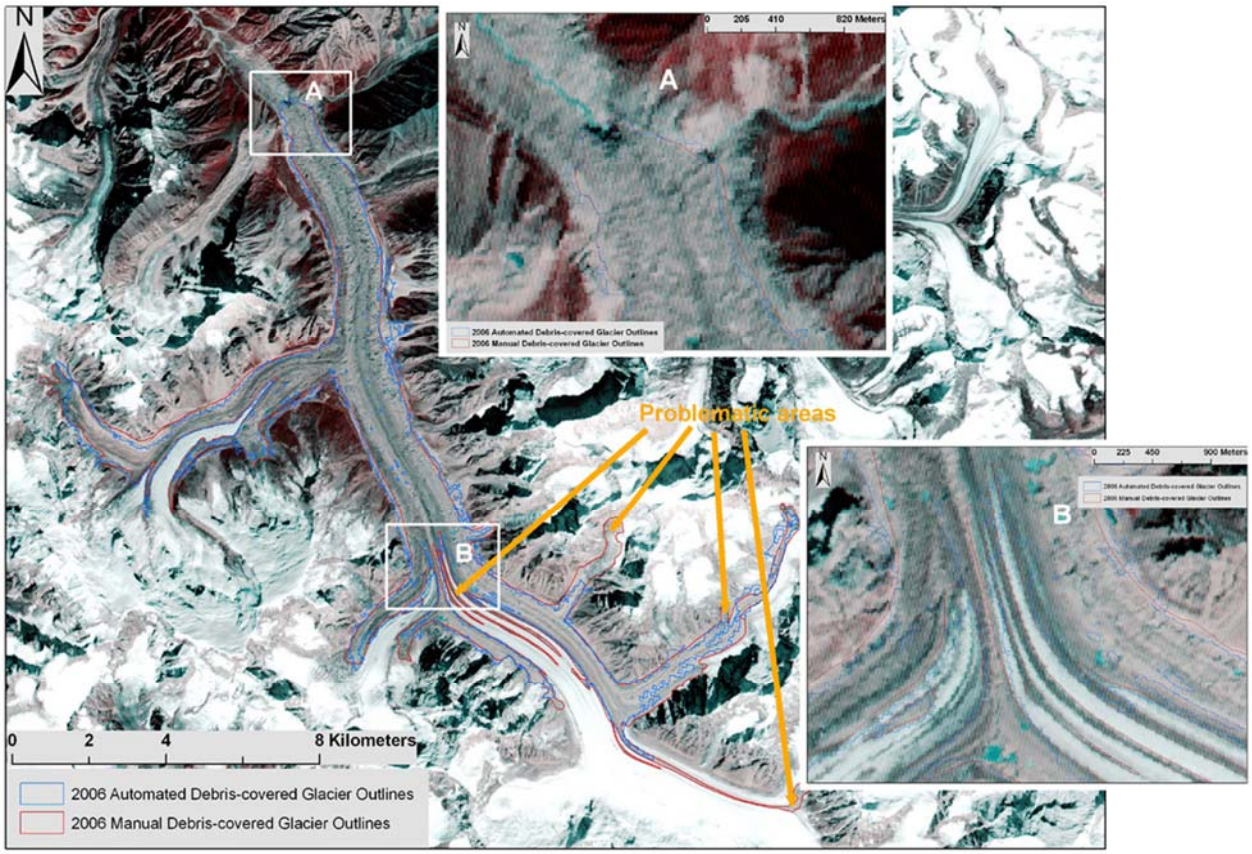

Figure 9 Comparison between automated and manually digitized outlines of the Gangotri Glacier.

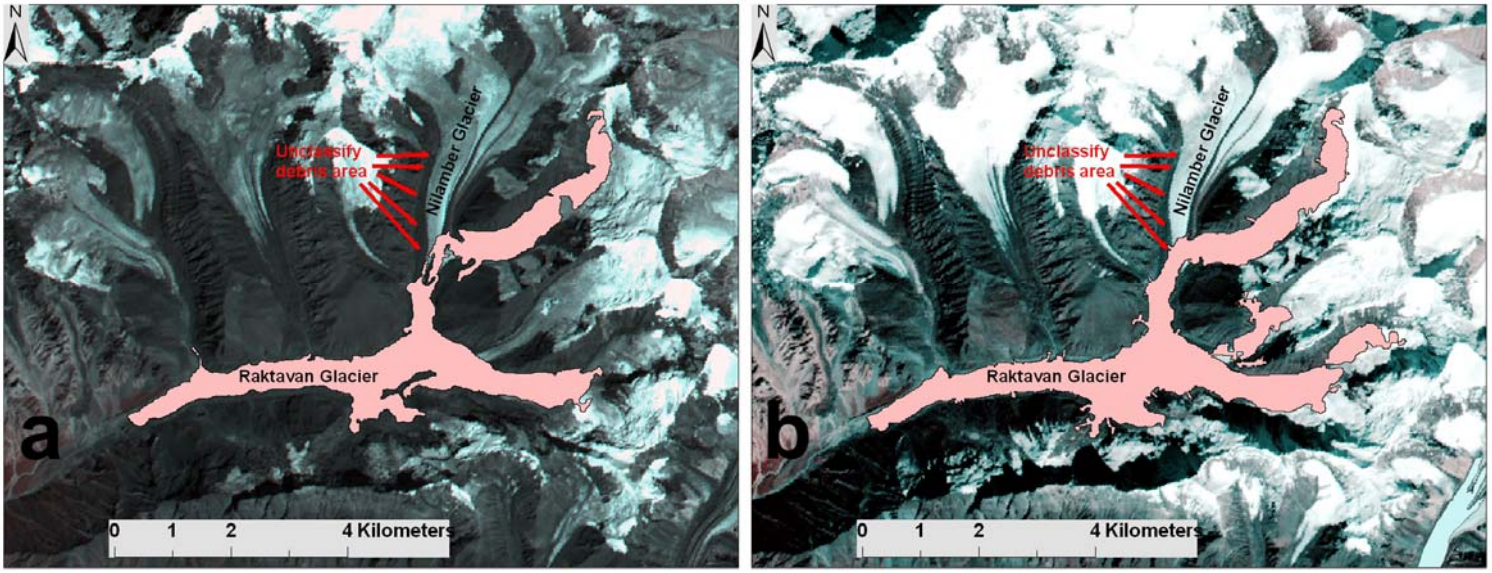

Figure 10 Reclassified cluster analysis in pink color based on (*a*) 2001 and (*b*) 2006 ASTER DEM overlaid on ASTER Image.

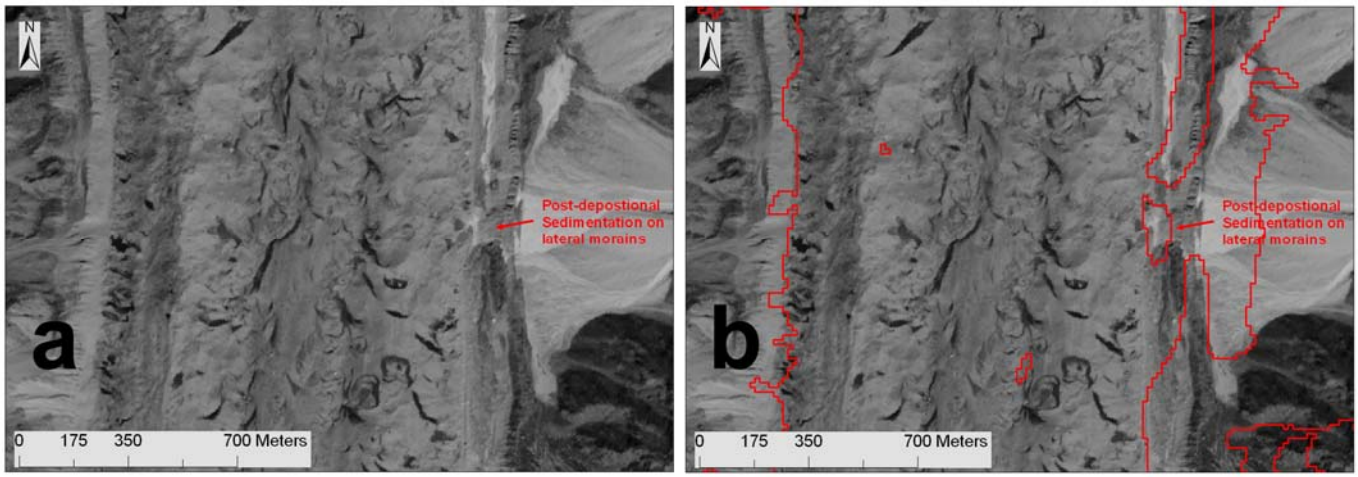

Figure 11(*a*) Cartosat-I image, (*b*) Vector layer derived from reclassified cluster analysis overlaid on Cartosat-I image.

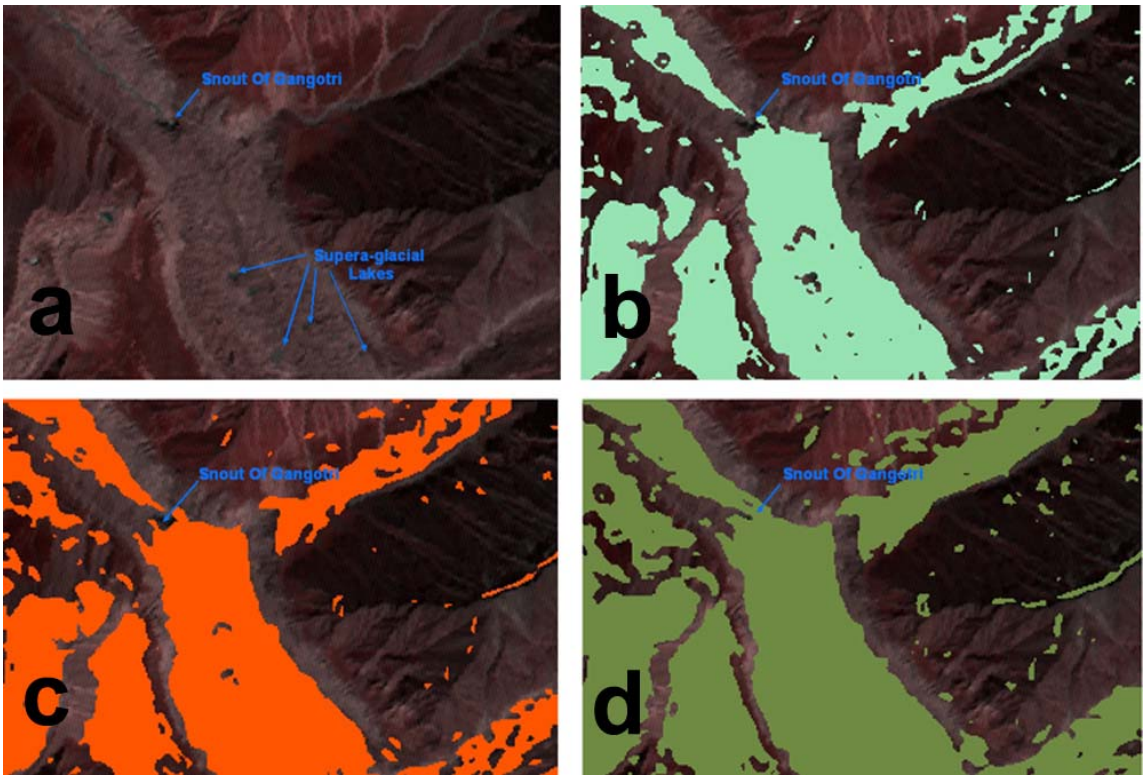

Figure 12 Average optimum slope calculations from ASTER DEM for Gangotri glacier (*a*) FCC of ASTER image, (*b*) 15 degree slope (light green colour), (*c*) 18 degree slope (orange colour), (*d*) 25 degree slope (dark green colour)